

Received April 15, 2020, accepted May 18, 2020, date of publication May 21, 2020, date of current version June 4, 2020.

Digital Object Identifier 10.1109/ACCESS.2020.2996278

Experimental Study on Glass and Polymers: Determining the Optimal Material for Potential Use in Terahertz Technology

MD SAIFUL ISLAM^{1,2}, (Member, IEEE), CRISTIANO M. B. CORDEIRO^{2,3}, MD J. NINE⁴, JAKEYA SULTANA¹, ALICE L. S. CRUZ⁵, ALEX DINOVTSEV¹, (Member, IEEE), BRIAN WAI-HIM NG¹, (Member, IEEE), HEIKE EBENDORFF-HEIDEPRIEM², DUSAN LOSIC⁴, AND DEREK ABBOTT¹, (Fellow, IEEE)

¹School of Electrical & Electronic Engineering, The University of Adelaide, Adelaide, SA 5005, Australia

²Institute for Photonics & Advanced Sensing, The University of Adelaide, Adelaide, SA 5005, Australia

³Institute of Physics, University of Campinas, Campinas 13083-859, Brazil

⁴School of Chemical Engineering & Advanced Materials, The University of Adelaide, Adelaide, SA 5005, Australia

⁵School of Electrical & Electronic Engineering, Braz Cubas University, Mogi das Cruzes-SP 08773-380, Brazil

Corresponding author: Md. Saiful Islam (mdsaiful.islam@adelaide.edu.au)

This work was supported by the Australian Research Council under Grant DP170104984. The work of Cristiano M. B. Cordeiro was supported by the Sao Paulo Research Foundation (FAPESP) under Grant 2018/10409. The work of Md J. Nine and Dusan Losic was supported by the Australian Research with the grant ARC Research Hub for Graphene Enabled Industry Transformation, funding under Industrial Transformation Research Hub under Grant IH150100003. The work of Heike Ebendorff-Heidepriem was supported by the Optofab node of the Australian National Fabrication Facility (ANFF) and the Commonwealth and South Australian State Government.

ABSTRACT The optical properties of polymers and glasses useful for terahertz applications are experimentally characterized using terahertz time-domain spectroscopy (THz-TDS). A standard system setup utilizing transmission spectroscopy is used to measure different optical properties of materials including refractive index, relative permittivity, loss tangent, absorption coefficient, and transmittance. The thermal and chemical dependencies of materials are also studied to identify the appropriate materials for given terahertz applications. The selected materials can then be utilized for applications such as in waveguides, filters, lenses, polarization preserving devices, metamaterials and metasurfaces, absorbers, and sensors in the terahertz frequency range.

INDEX TERMS Spectroscopy, terahertz materials, materials preparation, absorption, chemical analysis, thermal analysis.

I. INTRODUCTION

The terahertz spectrum (0.1–10 THz) is considered as one of the least explored segments in the electromagnetic spectrum due to the lack of powerful terahertz sources and efficient detectors. However, the recent technological advancements in optics and electronics, advances in terahertz systems utilizing mode-locked femtosecond fiber lasers, together with advances in emitters and receivers, have led to progress in this field [1]. The use of terahertz transmission mode has a number of significant applications spectroscopy [2], lenses [3], security [5], bio-imaging [6], photonic crystals [7]–[9], high bandwidth communications [10] and biological sensing [11]–[13]. One of the emerging applications of terahertz spectroscopy is to characterize the optical properties of a wide

variety of materials such as semiconductors, ceramics, chemical mixtures, gases, lubricating oils, glasses and polymers [1], [14]. There are particular advantages of using terahertz for material characterization. First, terahertz spectroscopy typically covers a very wide bandwidth and a large number of materials have spectral fingerprints within this frequency range. Second, terahertz spatial resolution is higher than microwaves because of its shorter wavelength, and finally, many dry non-polar materials are transparent to terahertz, making *in situ* characterization through packaging materials an attractive possibility [29].

Many materials were previously studied using far-infrared Fourier Transform Spectroscopy (FTS) where continuous wave (CW) non-coherent sources were used instead of the picosecond pulsed coherent sources in THz-TDS. There are a number of important aspects where THz-TDS differs from FTS that lends THz-TDS some significant advantages. The

The associate editor coordinating the review of this manuscript and approving it for publication was Jenny Mahoney.

measurements typically carried out with THz-TDS utilize a pump-probe configuration, where amplitude and phase are acquired simultaneously. The pump-probe detection scheme also has improved signal to noise ratio (up to 60 dB or 10^6 in power) compared to about 300 typically obtained using FTS [29].

Note that for material characterization, the absorption coefficient and refractive index are directly related to the transmitted signal amplitude and phase that are readily obtained using THz-TDS whereas FTS is only able to provide a field intensity measurement that can only provide the absorption coefficient, and refractive index can only be obtained indirectly by resorting to the Kramers-Kronig relation with reduced accuracy. Moreover, the high dynamic range of THz-TDS allows transmission studies of highly absorptive materials.

Measurement using THz-TDS falls into two distinct categories, one is to identify or differentiate substances contained in a material, and another is to characterize the optical and dielectric properties of materials. In 1990, a study on different highly resistive dielectrics and semiconductors including sapphire, quartz, silicon, germanium, gallium arsenide, etc. were carried out using far infrared, time-domain spectroscopy [15]. The refractive index and power absorption coefficients were measured within the frequency range of 0.2 to 2.0 THz. In 2011, Anthony *et al.* performed an analysis on Zeonex based microstructured fiber where the reported refractive index and absorption coefficients are 1.519 and 0.19 cm^{-1} respectively [18]. In 2007, Naftaly *et al.* carried out a study on polymers, oils and glasses [16]. However, they did not consider some important terahertz materials such as Zeonex, Topas, Teflon, PMMA, Duran and UV-resins, that are now commonly employed in various terahertz applications. In their analysis, Naftaly *et al.* showed that PMMA and HDPE achieve a refractive index of 1.61 and 1.54, where the reported absorption coefficients of these two materials are 7.5 and 0.225 cm^{-1} , respectively. Recently, Shi *et al.* [17] performed an optical and electrical characterization on PMMA for the application of broadband absorbers. In 2012, an experiment on different polymer materials was also carried out [35], where a refractive index of 1.61, and 1.54 for PMMA and HDPE having corresponding absorption coefficients of 7.5 , and 0.225 cm^{-1} respectively were obtained. Using transmission spectroscopy and S-parameters, Chang *et al.* also carried out studies on polymers at low (0.75–1.6 THz) frequencies. In 2011, Cunningham *et al.* also studied various polymers, however, they did not consider Zeonex, UV-resin nor any of the glasses [30]. In a 2014 spectroscopic study of common polymers, the authors did not consider some important terahertz materials such as Zeonex and HDPE [32]. Moreover, they did not consider glasses for characterization. Recently, in 2018, Pickwell-MacPherson's group carried out research on transparent, highly absorptive and conductive samples. In that work, they developed a fiber-based terahertz ellipsometer that provides excellent robustness on samples with different properties.

Recently, a fundamental study of THz-TDS measurements were carried out, however the authors did not present specific samples for study [33], [34]. More importantly none of the above referenced articles [16], [30], [32]–[34] consider the analysis of the thermal and chemical properties of materials.

Considering the importance of the characterization of the optical, thermal and chemical properties of polymers, glasses and UV-resins, in this paper we introduce a combined characterization approach aimed at assisting the selection of the most appropriate materials for various terahertz applications. A comprehensive range of characterization methods is selected to provide the thermal range, chemical stability, absorption coefficients, transparency and loss properties for this purpose. The methods used for characterization are presented in the experimental section showing the experimental set-up and theoretical aspects of the required calculation. Finally, an overall performance analysis is carried out, together with a concise summary of material properties in the conclusion. The studied glasses and polymers in this manuscript are commonly used for making different terahertz devices including waveguides [21], [22], sensors, filters [23], [24], lenses, metamaterials [25] and metasurfaces [12], [26] for different applications in the terahertz frequency range. Some UV-resins for example can be used in stereolithography (SLA) 3D printers making them an interesting material for building terahertz waveguides [27], [28].

II. SAMPLE PREPARATION

Samples of Topas (5013 L-10) and Zeonex (480R) grades were prepared from raw pellets. Initially, filaments of those materials were made using a Filabot EX2 filament Extruder and used for 3D printing of the samples. Fused Deposition Modeling (FDM) for 3D printing technology with high printing resolution was used to fabricate the samples, however, the outcomes were not satisfactory as there were numerous ridges on the surface, see Fig. 1(i), which potentially scatter the terahertz beam. Moreover, the fabricated samples were not optically transparent, with almost zero transmission measured using THz-TDS due to numerous air voids.

In the second trial we put the pellets inside a metal holder placed into a furnace at 200°C . After 24 hours, the small voids coalesce into larger air bubbles, shown in Fig. 1(ii). The air bubbles in the sample also scatter the terahertz beam and are therefore also unsuitable for material characterization. We further place the samples inside the furnace for another 24 hours, which removes all of the air bubbles. The samples are then cooled down and removed from the holder, and then cut and polished to make both the surfaces flat, smooth and parallel.

The polishing is graded using progressively finer silicon carbide (SiC) sandpaper, of grit sizes 120, 240, 320, 400, 800, 1200 and 2500 respectively. The samples are then given a final polish and smoothed using water based diamond suspension of $3 \mu\text{m}$ particle size. The polished and smoothed sample is shown in Fig. 1(iii). The sample of UV-resin is made using Stereolithography (SLA) 3D printing technology and

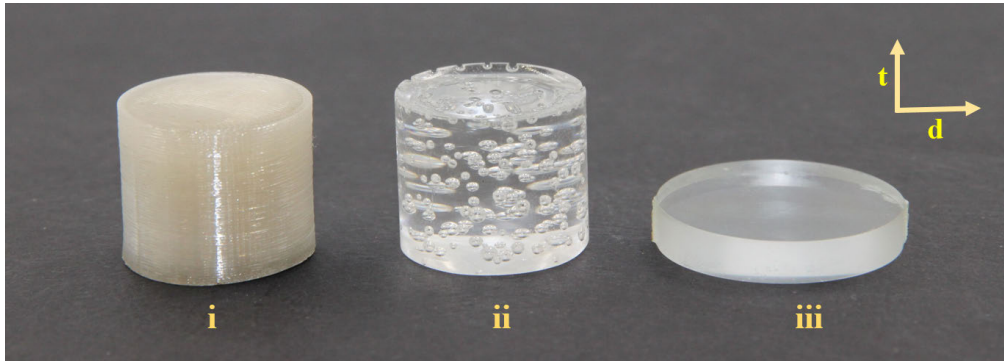


FIGURE 1. Different methodologies of preparing smoothed surfaced transparent Zeonex samples; (i) prepared using a 3D printer where the surface is rough containing ridges that potentially scatter the time domain signal, (ii) made using furnace at a temperature of 200°C for 24 hours, containing air bubbles, (iii) transparent sample without air bubbles inside, furnace at 200°C for 48 hours and polished with silicon carbide (SiC) sandpaper of different grit sizes. The d and t in the figure indicate the diameter and thickness of the samples which are 10mm×10mm for (i), 10mm×12mm for (ii), and 10mm×3mm for (iii).

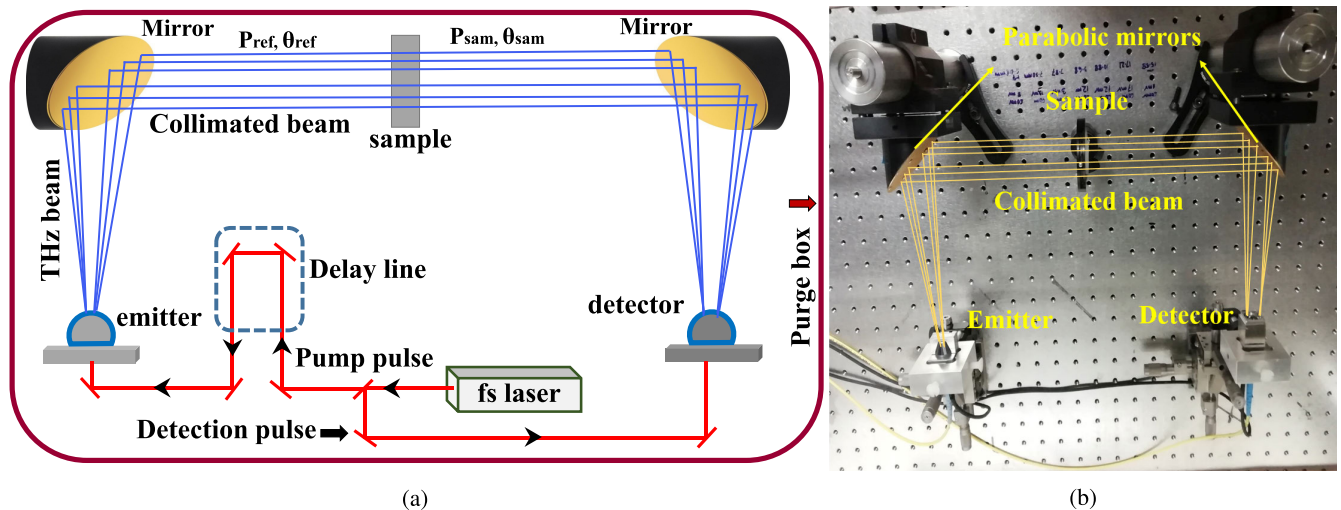


FIGURE 2. Schematic of experimental set-up of the enclosed THz-TDS system with a purge box filled with nitrogen, two parabolic mirrors creating a parallel beam where a sample holder is used to hold the sample, the reference signal (P_{ref} and θ_{ref}) is obtained by removing the samples whereas the sampled signal (P_{sam} and θ_{sam}) is obtained when a sample is in place as shown in the photograph, (b) the actual set-up.

polished before the experiment. Note that all other samples are cut and polished using the same procedure and all the measured samples have similar thickness of around 3 mm. Note that, the pellets of Topas and Zeonex are obtained from Zeon corporation, Japan. The UV-resin is prepared in Brazil, the sample of Teflon, PMMA, and HDPE are provided by the National T-ray facility lab, University of Adelaide. All the glass samples are supplied by the Institute for Photonics and Advanced Sensing (IPAS), University of Adelaide, Australia.

III. EXPERIMENTAL SETUP

The experimental setup and schematic are shown in Fig. 2a and Fig. 2b. This uses a dual-channel ultrashort pulse laser (Advantest TAS7400TS) with a pulse width of ≤ 50 fs (using 1.5m fiber), employing a simple configuration for fiber-coupled, free space terahertz generation and detection. The laser center wavelength, output power, and repetition rate is 1550 nm, ≥ 20 mW, and 50 MHz respectively.

In a phase modulated measurement method, the system time resolution is 2 fs, frequency resolution 1.9 GHz, scan range 524 ps, throughput 200 ms/scan and frequency accuracy is ± 10 GHz. The phase modulation measurement method relies on the difference in phase (arrival time) due to changes in wave path. The mechanical strain or thermal expansion of samples changes the optical path length and therefore cause changes in phase. This phases of reference and sample are then required to obtain the optical properties of the sample. The terahertz receiver Advantest model TAS1230 is fabricated with a photo-conductive antenna coupled to a hyper-hemispherical silicon lens in a fiber pigtailed compact housing. The transmitter utilizes the Cherenkov effect where the femtosecond optical pulse propagates through an electro-optic crystal with a second-order nonlinearity [36]. The Advantest model TAS1130 transmitter with a lithium niobate crystal waveguide has a bandwidth of 0.5 to 7 THz [37].

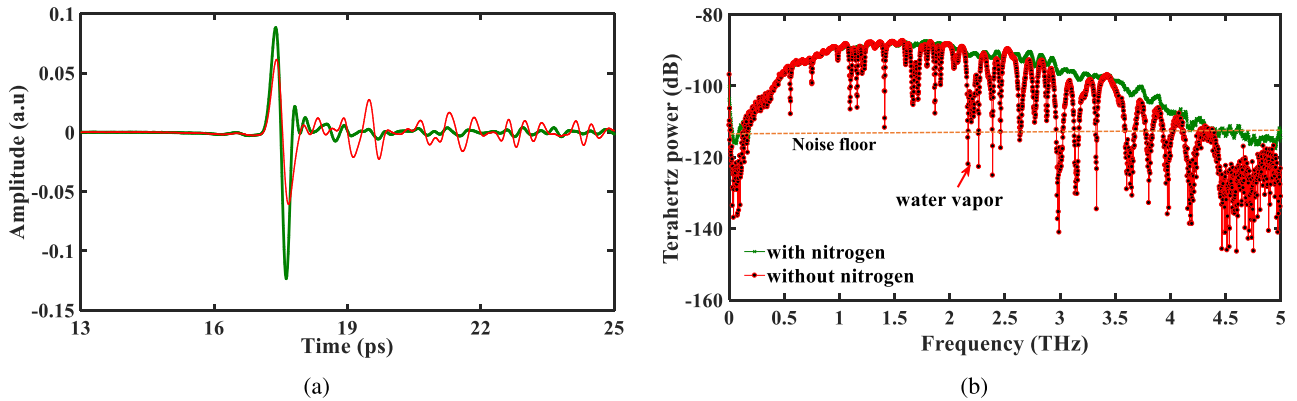


FIGURE 3. Effect of nitrogen, signal averaging and phase unwrapping. (a) Time-domain amplitude (a.u) and (b) power (dB), with and without dry nitrogen environment and signal averaging in the time domain. The red lines in the figures indicate signal without a nitrogen environment and averaging, whereas green lines indicate signal with nitrogen environment and averaging.

Two off-axis gold-coated parabolic mirrors (Edmund optics) with an effective focal length of 150 mm are used to create a parallel collimated beam for spectroscopy. To ensure the beam passing through the sample, we insert an iris of diameter less than the sample diameter. The reason for this standard setup is to obtain more averaged data from the measurements. In consideration to sample dimension, different types of sample holders were utilized to constrain the measurement to the sample and ensure consistent results. The system was enclosed with a custom made purge box and the performance with and without dry nitrogen are shown in Fig. 3a and Fig. 3b. It can be seen that without nitrogen and averaging (red) the terahertz amplitude (Fig. 3a) is comparatively reduced than in nitrogen environment and signal averaging (green). Moreover, for the spectrum (Fig. 3b) sharp water vapor lines are experienced, which is reduced in the nitrogen environment.

IV. SIGNAL PROCESSING TECHNIQUES: SIGNAL AVERAGING AND PHASE UNWRAPPING

The post-processing of THz-TDS data is followed by signal averaging and phase unwrapping. Random noise in measurements can be reduced by repeated multiple measurements. Signal averaging in the time domain, increases the signal strength relative to noise. Therefore, by averaging a set of replicated measurements, the signal to noise ratio (SNR) increases as a function of the square root of the number of ensembles [33]. In our case, we repeat the measurement having 2048 number of sample scanning. The result is depicted in Fig. 3a and Fig. 3b where signal amplitude and power are shown with signal averaging.

Phase unwrapping is a vital step for correct characterization of the optical constants of samples. The phase spectrum can be obtained from the transfer function that wraps around with an abrupt jump from $-\pi$ to π . This indicates that whenever the absolute value of the phase is greater than π , it will jump by 2π . Phase jumps create discontinuity artifacts in the phase spectrum, leading to the incorrect characterization of

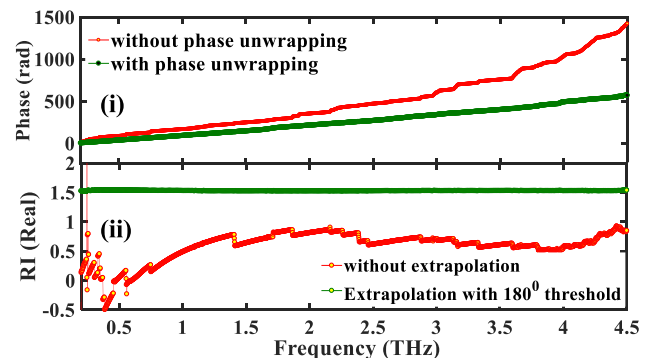


FIGURE 4. (i) The phase of the transfer function, obtained from the measurement of a Zeonex sample, is unwrapped with and without phase extrapolation. (ii) The index of refraction is determined by using the phases in (i). The reported value of the RI of Zeonex at terahertz frequencies is around 1.529.

optical properties. Phase unwrapping solves the phase wrapping problem. We choose a phase unwrap threshold of π and start unwrapping from 0.1 THz because at lower frequencies, errors in phase unwrapping can occur due to noise [33], [34].

The difference of phase of a transfer function obtained from a Zeonex sample by means of phase unwrapping and without phase unwrapping is shown in Fig. 4(i). This indicates that the phase extrapolation reduces phase jumps, making it suitable for correct sample characterization, even at very low frequencies. A complication of perfect phase unwrapping occurs at low and high frequencies where the noise plagues the amplitude and phase data, resulting in false unwrapping. Starting from noisy low frequencies, phase unwrapping causes error to propagate towards the phase at high frequencies. As a solution, an adaptive unwrapping procedure is followed that discards the phase at low frequencies. The missing phase profile at low frequencies is then extrapolated from high frequency unwrapped phases [33]. With phase unwrapped, the refractive index of Zeonex is characterized, as shown in Fig. 4(ii). This illustrates the large error in the refractive index without unwrapping, while phase

extrapolated by 180° corrects the refractive index measurement of Zeonex to the expected correct value of 1.529.

V. MATHEMATICAL EXPRESSIONS TO EXTRACT OPTICAL PROPERTIES FROM THz-TDS DATA

The received power spectrum, transmittance, absorption coefficient, phase shift, refractive index, dielectric loss and permittivity are calculated using the following expressions [37]

$$P_{\text{linear}}(\omega) = |\tilde{F}(\omega)|^2 \tag{1}$$

where $P_{\text{linear}}(\omega)$ indicate the linear power spectrum, $\tilde{F}(\omega)$ and $|\tilde{F}(\omega)| = \sqrt{\text{Re}(\tilde{F}(\omega))^2 + \text{Im}(\tilde{F}(\omega))^2}$ represents the FFT complex data and magnitude respectively. Now, the linear transmittance can be found from the below equation

$$T_{\text{linear}}(\omega) = \frac{P_{\text{sam}}(\omega)}{P_{\text{ref}}(\omega)} \times 100 \tag{2}$$

where $T_{\text{linear}}(\omega)$ indicates the transmittance, and $P_{\text{ref}}(\omega)$ and $P_{\text{sam}}(\omega)$ represents the reference and sample power spectrum.

The absorption coefficient of a sample can be represented as [16],

$$\alpha_{\omega} = \frac{2\omega k(\omega)}{c} \tag{3}$$

where, α_{ω} represents the absorption coefficient [m^{-1}], $k(\omega)$ represents the extinction coefficient, ω represents the angular frequency, [$\text{rad}/10^{-12}\text{s}$], and c represents the speed of light, [m/s].

The phase shift between the sampled and referenced signal can be denoted by [33],

$$\phi(\omega) = \theta_{\text{sam}}(\omega) - \theta_{\text{ref}}(\omega) \tag{4}$$

where $\phi(\omega)$, [rad], represents the phase shifts, $\theta_{\text{sam}}(\omega)$ and $\theta_{\text{ref}}(\omega)$ represents the sample and reference phases respectively.

Now, the refractive index $n(\omega)$ and extinction coefficient $k(\omega)$ of a sample can be represented as,

where $n(\omega)$ and $k(\omega)$ represents the refractive index and the extinction coefficients respectively, $\tilde{t}_{\text{sa}}(\omega) = \tilde{t}_{\text{as}}(\omega) = \frac{2}{\tilde{n}(\omega) + 1}$, $\tilde{r}_{\text{sa}}(\omega) = \tilde{r}_{\text{as}}(\omega) = \frac{\tilde{n}(\omega) - 1}{\tilde{n}(\omega) + 1}$, d represents the sample thickness, $\tilde{n}(\omega) = n(\omega) - ik(\omega)$ indicate the complex index of refraction, $\text{Arg}[\cdot] = \tan^{-1}(y/x)$ denotes the deflection angle, m indicates the number of multiple reflections. The deflection angle term can be neglected for thicker

samples and therefore we use a simplified form of Eqn. 5 to obtain the refractive indices, Eqn. 7.

In simplified form, neglecting the deflection angle, the refractive index and extinction coefficient can be written as [16], [33]

$$n(\omega) = 1 + \frac{c\phi(\omega)}{d\omega} \tag{7}$$

$$k(\omega) = -\frac{c}{d\omega} \left\{ \ln \left[\frac{4n(\omega)}{[n(\omega) + 1]^2} \right] - \ln |T_{\text{linear}}(\omega)| \right\} \tag{8}$$

Using the refractive index, the permittivity and the dielectric loss tangent can then be calculated by [37],

$$\varepsilon_1(\omega) = n(\omega)^2 - k(\omega)^2 \tag{9}$$

$$\varepsilon_2(\omega) = 2n(\omega)k(\omega) \tag{10}$$

where $\varepsilon_1(\omega)$ and $\varepsilon_2(\omega)$ represents the permittivity and dielectric loss tangent respectively.

VI. DIELECTRIC AND OPTICAL PROPERTIES OF MEASURED SAMPLES

At terahertz frequencies, the dielectric and optical properties including the refractive index, dielectric constant, bandwidth, absorption coefficient, dielectric loss, and transmittance of the samples is illustrated and discussed in this section. The measured terahertz power (dB) passing through various samples is shown in Fig. 5a. The system is purged and the measurements are carried out in a nitrogen environment. As compared to Fig. 3b (without nitrogen), we see that the water vapor peaks are significantly reduced in nitrogen environment, Fig. 5a. We see that a similar transmission bandwidth is obtained for Zeonex, Topas, HDPE, and Teflon where a comparatively lower transmission bandwidth is achieved for PMMA. From the glasses, the FS-300 Silica shows better power transmission over other measured glasses such as BK7 and Duran. The FS-300 Silica, BK7, and Duran achieve a transmission bandwidth of around 2.5 THz, 0.75 THz, and 1.1 THz respectively, while the UV-resin exhibits the narrowest power transmission bandwidth of all polymers at around 0.9 THz. Fig. 5a illustrates the water vapor peaks from the measurement environment and the nature of the samples itself that can be reduced by flushing the measurement system with dry nitrogen, and storing the samples in a dry environment.

The transmittance of the materials is calculated using Eq. 2 and illustrated in Fig. 5b, showing the low terahertz transmittance for BK7, UV-resin, Duran and silica, and better trans-

$$n(\omega) = 1 + \frac{c\phi(\omega)}{d\omega} + \frac{c}{d\omega} \text{Arg} \left[\tilde{t}_{\text{as}}(\omega)\tilde{t}_{\text{sa}}(\omega) \times \sum_{l=0}^m \left((\tilde{r}_{\text{sa}}(\omega))^2 \exp \left[-i \frac{2\tilde{n}(\omega)d\omega}{c} \right] \right)^l \right] \tag{5}$$

$$k(\omega) = -\frac{c}{2d\omega} \ln \left[\frac{T_{\text{linear}}(\omega)}{\left| \tilde{t}_{\text{as}}(\omega)\tilde{t}_{\text{sa}}(\omega) \times \sum_{l=0}^m \left((\tilde{r}_{\text{sa}}(\omega))^2 \exp \left[-i \frac{2\tilde{n}(\omega)d\omega}{c} \right] \right)^l \right|^2} \times \frac{1}{100} \right] \tag{6}$$

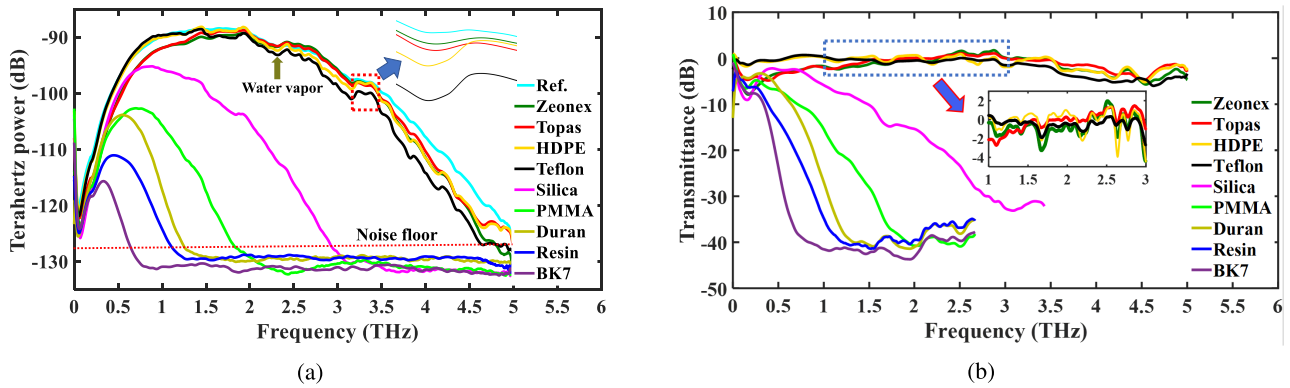


FIGURE 5. Spectral response and transmittance’s of the measured polymers and glasses. (a) The received power spectrum of reference (background), Zeonex, Topas, HDPE, Teflon, Silica, PMMA, BK7, Duran, and UV-resin, (b) The terahertz transmittance’s of the same materials.

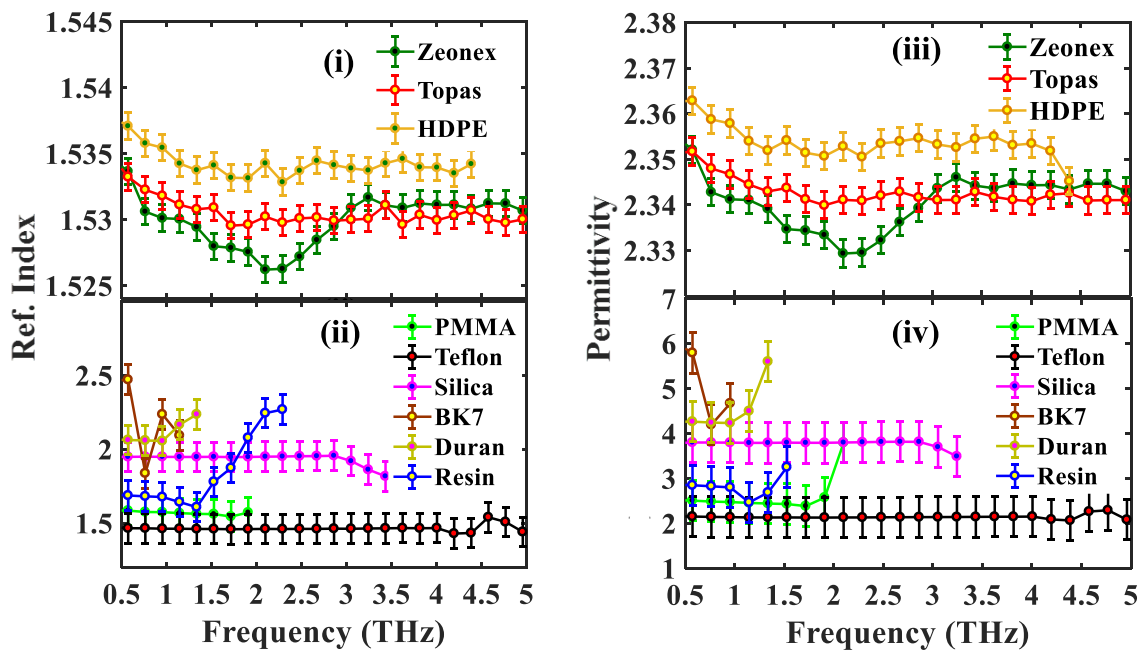


FIGURE 6. Refractive indices (i–ii), and dielectric constants (iii–iv) of the measured polymers and glasses.

mittances for Zeonex, Topas, Teflon, and HDPE. Therefore, a high-frequency application that requires high transparency, should utilize the Zeonex, Topas, HDPE and Teflon materials wherever their mechanical and thermal properties may allow this.

Using the time delays of measured samples, the associated phases are extracted. This data, together with the phases and extinction coefficients, enables the calculation of refractive indices and relative permittivities, as illustrated in Fig. 6 (i-ii) and Fig. 6 (iii-iv). The average refractive index of the measured Zeonex, Topas, HDPE, PMMA, Teflon, Silica, BK7, Duran, and Resin are 1.529, 1.531, 1.535, 1.584, 1.466, 1.943, 2.46, 2.06, and 1.69 respectively. The relative permittivities has a square relation with the refractive index. The measured properties are compared with the literature [14], [16], [29], [30], shown in Tab. 1, which are perfectly matched.

The absorption coefficients and dielectric loss tangents of the measured samples are illustrated in Fig. 7 (i–ii) and Fig. 7 (iii–iv). These are higher for all the glasses, PMMA and UV-resin than for Zeonex, Topas, HDPE, and Teflon. However, Fig. 7 also illustrate that the absorption coefficient and loss tangent for HDPE and Teflon are relatively higher at high frequencies than Zeonex and Topas. The obtained average absorption coefficients and loss tangents are summarized in Tab. 1 and compared with the literature. Note that Topas and Zeonex show almost similar properties all over the frequency of interests. The unwanted peaks in the absorption spectrum are due to the remained water vapor present during measurements.

In Tab. 1 we combine the properties including refractive indices, relative permittivities, loss tangents and absorption coefficients of the measured glasses and polymers. These

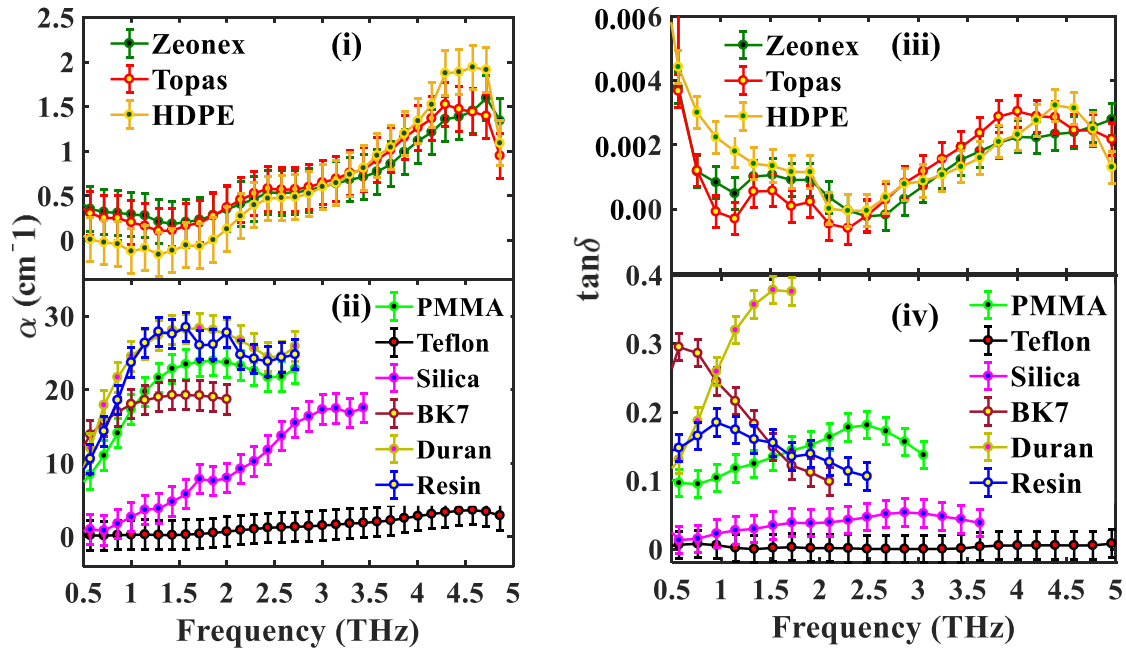


FIGURE 7. (i-ii) Absorption coefficients, and (iii-iv) dielectric loss tangents of the measured polymers and glasses showing low absorption coefficients for the polymers than the glasses and UV-resin.

TABLE 1. Comparative study of refractive indices, relative permittivities, loss tangents, and absorption coefficients of the measured samples with the literature.

Sample	n (measured) (average)	n (published)	Relative permittivities	Dielectric loss tangents, (tanδ)	α (cm ⁻¹) (measured)	α (cm ⁻¹) (published)
Zeonex	1.529	1.519 [18]	2.34	0.006	0.184	0.19 [18]
Topas	1.531	1.53 [35], 1.525 [30]	2.343	0.007	0.20	0.15 [35], 0.25 [30]
PMMA	1.584	1.61 [16], 1.57 [30]	2.50	0.10	4.40	7.5 [16], 9.25 [30]
HDPE	1.535	1.54 [16], 1.36 [35]	2.36	0.005	0.22	0.225 [16], 1.66 [35]
Teflon	1.466	1.45 [30], 1.42 [35]	2.15	0.008	0.26	0.25 [30], 0.6 [35]
TPX	-	1.455 [39]	2.11	-	-	0.4 [39]
PP	-	1.48 [40]	2.19	-	-	0.29 [40]
Silica	1.943	1.96 [16]	3.78	0.045	1.98	3.5 [16], 3.8 [19]
BK7	2.46	2.52 [16]	6.05	0.21	11	15 [20]
Duran	2.06	-	4.05	0.25	15	-
UV-resin	1.69	-	2.86	0.15	16	-

properties are then compared with the literature and it can be seen that they are in good agreements.

In addition to searching for the low loss materials from the studied glasses and polymers, it is also necessary to characterize their thermal and chemical stabilities. Therefore besides the optical properties, we also determine the thermal and chemical properties of the low loss polymers to find out the suitable materials to be applicable in harsh and hostile environments.

VII. CHEMICAL AND THERMAL STABILITY OF THE LOW LOSS POLYMERS

To measure the chemical stability, as in Fig. 8, 0.5 g of each material was exposed to 10 ml of highly acidic (low pH) H₂SO₄ (10 M) solution, saline NaCl (3.5 M) solution, and basic (high pH) NaOH (10 M) solution (here, M indicates molar concentration). These solutions were agitated by a mechanical shaker at 200 rpm for 24 hrs to observe any effect of a chemical attack on the materials. No physical changes

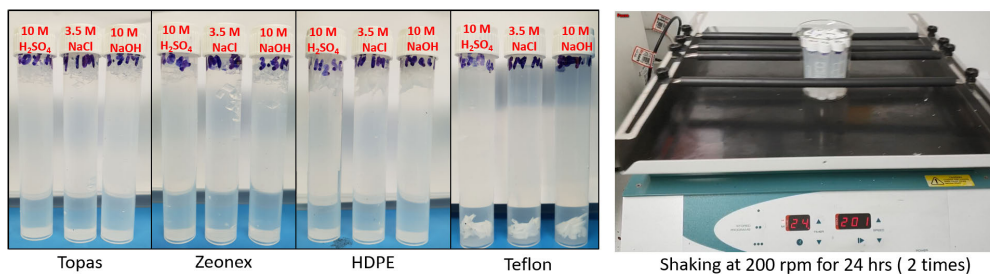


FIGURE 8. Chemical stability testing of Topas, Zeonex, HDPE and Teflon over acidic, salinic, and basic environments.

TABLE 2. The onset temperature, peak temperature, and the difference between onset and peak temperature of HDPE, Teflon, Topas and Zeonex at a heating rate of 5°C/min.

Sample	Onset Temperature (°C)	Peak Temperature (°C)	ΔT (°C)
HDPE	468	485	17
Teflon	580	610	30
Topas	460	476	16
Zeonex	443	463	20

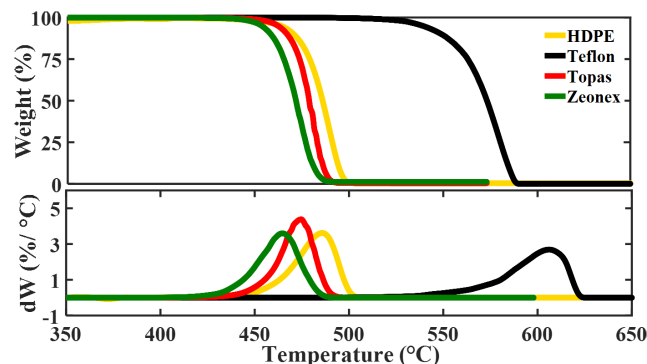


FIGURE 9. Percentage of weight loss and derivative of weight loss of HDPE, Topas, Teflon, and Zeonex as a function of temperature variation.

were observed in the first 24 hrs, thus the agitation was continued for another round of 24 hrs. Finally, the materials were taken out and dried at room temperature followed by a mass measurement. No significant mass change ($\pm 1.5\%$) was measured for any of these four materials which demonstrates the extreme chemical stability of these materials against acidic, saline and basic environment.

In order to characterize the thermal stability of the selected materials (Topas, Zeonex, HDPE, Teflon), the thermogravimetric (TG) and derivative thermogravimetric (DTG) analysis were carried out using non-isothermal thermogravimetric analysis setup, TA Instruments (Q-500, Tokyo, Japan). The thermal analyzer was temperature calibrated between experiments using the Curie point of nickel as a reference. The experiment is performed under a nitrogen environment at a purge rate of 60 ml/min. For each polymer, samples of approximately 40 mg was heated upto 800°C at a heating rate of 5°C/min. Based on the heating rate the onset temperature and peak temperature may vary however for the simplicity of analysis we consider a heating rate of 5°C/min. The TG and DTG curves for HDPE, Teflon, Topas and Zeonex is illustrated in Fig. 9 where the DTG plot shows a peak weight loss from where the peak temperature degradation (T_p) can be determined. The onset temperature degradation (T_{onset}) is the point at which the material starts to degrade or disintegrate while the peak temperature is a point at which the degradation rate reaches at its maximum. The detail of thermal characteristics of the samples including the weight loss temperatures, T_p and T_{onset} is shown in Tab. 2.

According to Tab. 2 and Fig. 9 we find that the Teflon has highest thermal stability among the experimented samples and starts losing its weight due to evaporation from around 525°C and ended up at around 620°C. While the other three materials HDPE, Topas, and Zeonex have shown similar thermal characteristics and start losing weight from 440°C and ending up of around 480 to 500°C. Fig. 9 also illustrates that all the samples lose their weight after a particular temperature is attained, and the obtained results are aligned with a previous thermal study of Topas and HDPE [38].

Though Teflon has the best thermal stability, it shows higher absorption loss and dielectric loss tangent at high frequencies compared to Zeonex, Topas and HDPE. Teflon is a fairly heat resistant and excellent anti-friction polymer that enables its use in mechanical units without additional lubrication. High loss materials such as PMMA, Silica, BK7, Duran, resin, etc. also have high refractive indices that can be used for thinner metamaterial or metasurface designs. Moreover, crystalline materials such as silicon, germanium, sapphire and quartz demonstrate low transmittance at terahertz due to reflection losses. The absorption coefficients of these materials are around 0.5 cm^{-1} [41], [42]. Because of the high refractive index and desired physiochemical properties, these crystalline materials are widely used in manufacturing substrates with high-quality interference mirrors with high reflection coefficients. As demonstrated in Fig. 9, HDPE shows improved thermal stability over Zeonex or Topas, however, HDPE has higher absorption loss. Similar to Teflon,

HDPE exhibits an increasing loss trend at higher frequencies. The thin HDPE films are used for manufacturing terahertz polarizers and windows for Golay cells. The absorption coefficient, dielectric loss tangent, transmittance and thermal stability of Zeonex and Topas are almost identical, with a linear trend in optical characteristics, observed at higher terahertz frequencies. The absorption coefficient and loss tangent of Zeonex and Topas are extremely low and that also comes with higher transmittance than any other measured samples. Other polymers such as polypropylenes (PP) and polymethylpentene (TPX) show potential for terahertz applications however both have higher absorption coefficients (0.29 cm^{-1} @ 1.0 THz for PP, and $\sim 0.4 \text{ cm}^{-1}$ @ 1.0 THz, for TPX) [39], [40] than Topas and Zeonex. Low loss TPX is a strong material and can mechanically be converted into lenses and windows, exhibiting excellent optical properties for serving as an ideal substitute for picarin (tsurupica) in the manufacture of lenses. Picarin is commercially less accessible and more expensive [35]. However, based on transparency and absorption coefficients, the Zeonex and Topas as considered as improvements over TPX. Therefore, in consideration of absorption coefficients, transparency, dielectric loss tangents and thermal and chemical stabilities of the polymer materials, Zeonex and Topas can be considered as desirable for applications in terahertz technology. These applications include terahertz lenses, modulators, filters, metamaterials, metasurfaces and terahertz sensors.

VIII. CONCLUSION

The optical, chemical and thermal properties of glasses and polymers are investigated to select the optimal materials for applications in terahertz technology. The THz-TDS and TGA analyses are carried out for obtaining optical and thermal properties whereas the experiments of chemical properties are carried out in acidic, saline and basic environments. Optical, thermal and chemical investigations show that the materials are highly chemically and thermally stable. However, considering the absorption coefficients, transmittances and loss tangents, both Zeonex and Topas are found to be best suited for terahertz applications.

ACKNOWLEDGMENT

The authors would like to thank the support of Mr. Alson from Institute for Photonic and Advanced Sensing (IPAS) for his support during sample preparation.

REFERENCES

- [1] B. Ferguson and X.-C. Zhang, "Materials for terahertz science and technology," *Nature Mater.*, vol. 1, no. 1, pp. 26–33, Sep. 2002.
- [2] G. Zhao, G. Savini, Y. Yu, S. Li, J. Zhang, and P. Ade, "A dual-port THz time domain spectroscopy system optimized for recovery of a sample's Jones matrix," *Sci. Rep.*, vol. 9, no. 1, p. 2099, Dec. 2019.
- [3] J. He, J. Ye, X. Wang, Q. Kan, and Y. Zhang, "A broadband terahertz ultrathin multi-focus lens," *Sci. Rep.*, vol. 6, no. 1, p. 28800, Jun. 2016.
- [4] J. Ma, R. Shrestha, J. Adelberg, C.-Y. Yeh, Z. Hossain, E. Knightly, J. M. Jornet, and D. M. Mittleman, "Security and eavesdropping in terahertz wireless links," *Nature*, vol. 563, no. 7729, pp. 89–93, Nov. 2018.
- [5] X. Deng, L. Li, M. Enomoto, and Y. Kawano, "Continuously frequency-tunable plasmonic structures for terahertz bio-sensing and spectroscopy," *Sci. Rep.*, vol. 9, no. 1, p. 3498, Dec. 2019.
- [6] Z. Xu and E. Y. Lam, "Hyperspectral reconstruction in biomedical imaging using terahertz systems," in *Proc. IEEE Int. Symp. Circuits Syst.*, vol. 9, May 2010, pp. 2079–2082.
- [7] W. Withayachumnankul, M. Fujita, and T. Nagatsuma, "Integrated silicon photonic crystals toward terahertz communications," *Adv. Opt. Mater.*, vol. 6, no. 16, Aug. 2018, Art. no. 1800401.
- [8] M. S. Islam, J. Sultana, K. Ahmed, M. R. Islam, A. Dinovitser, B. W.-H. Ng, and D. Abbott, "A novel approach for spectroscopic chemical identification using photonic crystal fiber in the terahertz regime," *IEEE Sensors J.*, vol. 18, no. 2, pp. 575–582, Jan. 2018.
- [9] M. S. Islam, J. Sultana, A. Dinovitser, B. W.-H. Ng, and D. Abbott, "A novel Zeonex based oligoporous-core photonic crystal fiber for polarization preserving terahertz applications," *Opt. Commun.*, vol. 413, pp. 242–248, Apr. 2018.
- [10] J. F. O'Hara, S. Ekin, W. Choi, and I. Song, "A perspective on terahertz next-generation wireless communications," *Technologies*, vol. 7, no. 2, p. 43, Jun. 2019.
- [11] X. Chen, W. Fan, and C. Song, "Multiple plasmonic resonance excitations on graphene metamaterials for ultrasensitive terahertz sensing," *Carbon*, vol. 133, pp. 416–422, Jul. 2018.
- [12] M. S. Islam, J. Sultana, M. Biabanifard, Z. Vafapour, M. J. Nine, A. Dinovitser, C. M. B. Cordeiro, B. W.-H. Ng, and D. Abbott, "Tunable localized surface plasmon graphene metasurface for multiband superabsorption and terahertz sensing," *Carbon*, vol. 158, pp. 559–567, Mar. 2020.
- [13] A. Keshavarz and Z. Vafapour, "Sensing avian influenza viruses using terahertz metamaterial reflector," *IEEE Sensors J.*, vol. 19, no. 13, pp. 5161–5166, Jul. 2019.
- [14] M. C. Beard, G. M. Turner, and C. A. Schmuttenmaer, "Subpicosecond carrier dynamics in low-temperature grown GaAs as measured by time-resolved terahertz spectroscopy," *J. Appl. Phys.*, vol. 90, no. 12, pp. 5915–5923, Dec. 2001.
- [15] D. Grischkowsky, S. Keiding, M. van Exter, and C. Fattinger, "Far-infrared time-domain spectroscopy with terahertz beams of dielectrics and semiconductors," *J. Opt. Soc. Amer. B, Opt. Phys.*, vol. 7, no. 10, pp. 2006–2015, 1990.
- [16] M. Naftaly and R. E. Miles, "Terahertz time-domain spectroscopy for material characterization," *Proc. IEEE*, vol. 95, no. 8, pp. 1658–1665, Aug. 2007.
- [17] Z. Shi, L. Song, and T. Zhang, "Optical and electrical characterization of pure PMMA for terahertz wide-band metamaterial absorbers," *J. Infr. Millim., Terahertz Waves*, vol. 40, no. 1, pp. 80–91, Jan. 2019.
- [18] J. Anthony, R. Leonhardt, A. Argyros, and M. C. J. Large, "Characterization of a microstructured Zeonex terahertz fiber," *J. Opt. Soc. Amer. B, Opt. Phys.*, vol. 28, no. 5, pp. 1013–1018, 2011.
- [19] F. Sanjuan and J. O. Tocho, "Optical properties of silicon, sapphire, silica and glass in the Terahertz range," in *Latin Amer. Opt. Photon. Conf., OSA Tech. Dig.* Washington, DC, USA: Optical Society America, 2012, pp. 1–4.
- [20] M. Naftaly and R. E. Miles, "Terahertz time-domain spectroscopy of silicate glasses and the relationship to material properties," *J. Appl. Phys.*, vol. 102, no. 4, Aug. 2007, Art. no. 043517.
- [21] M. S. Islam, J. Sultana, S. Rana, M. R. Islam, M. Faisal, S. F. Kaijage, and D. Abbott, "Extremely low material loss and dispersion flattened TOPAS based circular porous fiber for long distance terahertz wave transmission," *Opt. Fiber Technol.*, vol. 34, pp. 6–11, Mar. 2017.
- [22] M. S. Islam, S. Rana, M. R. Islam, M. Faisal, H. Rahman, and J. Sultana, "Porous core photonic crystal fibre for ultra-low material loss in THz regime," *IET Commun.*, vol. 10, no. 16, pp. 2179–2183, Nov. 2016.
- [23] H. Li, S. Atakaramians, J. Yuan, H. Xiao, W. Wang, Y. Li, B. Wu, and Z. Han, "Terahertz polarization-maintaining subwavelength filters," *Opt. Express*, vol. 26, no. 20, pp. 25617–25629, 2016.
- [24] F. Pavanello, F. Garet, M.-B. Kuppam, E. Peytavit, M. Vanwollegem, F. Vaurette, J.-L. Coutaz, and J.-F. Lampin, "Broadband ultra-low-loss mesh filters on flexible cyclic olefin copolymer films for terahertz applications," *Appl. Phys. Lett.*, vol. 102, no. 11, Mar. 2013, Art. no. 111114.
- [25] X. He, "Tunable terahertz graphene metamaterials," *Carbon*, vol. 82, pp. 229–237, Feb. 2015.
- [26] R. T. Ako, A. Upadhyay, W. Withayachumnankul, M. Bhaskaran, and S. Sriram, "Dielectrics for terahertz metasurfaces: Material selection and fabrication techniques," *Adv. Opt. Mater.*, vol. 8, no. 3, Feb. 2020, Art. no. 1900750.

- [27] A. L. S. Cruz, C. M. B. Cordeiro, and M. A. R. Franco, "Microstructures in polymer fibres for optical fibres, THz waveguides, and fibre-based metamaterials," *ISRN Opt.*, vol. 2013, Feb. 2013, Art. no. 785162.
- [28] A. L. S. Cruz, C. Cordeiro, and A. R. M. Franco, "3D printed hollow-core terahertz fibers," *Fibers*, vol. 6, no. 3, 2018, Art. no. 43.
- [29] P. H. Bolivar, M. Brucherseifer, J. G. Rivas, R. Gonzalo, I. Ederra, A. L. Reynolds, M. Holker, and P. de Maagt, "Measurement of the dielectric constant and loss tangent of high dielectric-constant materials at terahertz frequencies," *IEEE Trans. Microw. Theory Techn.*, vol. 51, no. 4, pp. 1062–1066, Apr. 2003.
- [30] P. D. Cunningham, N. N. Valdes, F. A. Vallejo, L. M. Hayden, B. Polishak, X.-H. Zhou, J. Luo, A. K.-Y. Jen, J. C. Williams, and R. J. Twieg, "Broadband terahertz characterization of the refractive index and absorption of some important polymeric and organic electro-optic materials," *J. Appl. Phys.*, vol. 109, no. 4, Feb. 2011, Art. no. 043505.
- [31] T. Chang, X. Zhang, X. Zhang, and H.-L. Cui, "Accurate determination of dielectric permittivity of polymers from 75 GHz to 1.6 THz using both S-parameters and transmission spectroscopy," *Appl. Opt.*, vol. 56, no. 12, pp. 3287–3292, 2017.
- [32] F. D'Angelo, Z. Mics, M. Bonn, and D. Turchinovich, "Ultra-broadband THz time-domain spectroscopy of common polymers using THz air photonics," *Opt. Express*, vol. 22, no. 10, pp. 12475–12485, 2014.
- [33] W. Withayachumnankul and M. Naftaly, "Fundamentals of measurement in terahertz time-domain spectroscopy," *J. Infr., Millim., Terahertz Waves*, vol. 35, no. 8, pp. 610–637, Aug. 2014.
- [34] P. U. Jepsen, "Phase retrieval in terahertz time-domain measurements: A 'how to' tutorial," *J. Infr., Millim., Terahertz Waves*, vol. 40, no. 4, pp. 395–411, Apr. 2019.
- [35] E. V. Fedulova, M. M. Nazarov, A. A. Angeluts, M. S. Kitai, V. I. Sokolov, and A. P. Shkurinov, "Studying of dielectric properties of polymers in the terahertz frequency range," *Proc. SPIE*, vol. 8337, Feb. 2012, Art. no. 83370I, doi: 10.1117/12.923855.
- [36] D. H. Auston, K. P. Cheung, J. A. Valdmanis, and D. A. Kleinman, "Cherenkov radiation from femtosecond optical pulses in electro-optic media," *Phys. Rev. Lett.*, vol. 53, no. 16, pp. 1555–1558, Oct. 1984.
- [37] Advantest Corporation. *Terahertz, Wave Spectroscopy and Analysis Platform*. Accessed: Oct. 15, 2019. [Online]. Available: <https://www.advantest.com/products/terahertzspectroscopic-imaging-systems>
- [38] C. Liu, J. Yu, X. Sun, J. Zhang, and J. He, "Thermal degradation studies of cyclic olefin copolymers," *Polym. Degradation Stability*, vol. 81, no. 2, pp. 197–205, Jan. 2003.
- [39] A. Podzorov and G. Gallot, "Low-loss polymers for terahertz applications," *Appl. Opt.*, vol. 47, no. 18, pp. 3254–3257, 2008.
- [40] M. S. Kitai, M. M. Nazarov, P. M. Nedorezova, and A. P. Shkurinov, "Determination of the boundary transition temperatures in polypropylene on the basis of measurements in the terahertz band," *Radiophys. Quantum Electron.*, vol. 60, no. 5, pp. 409–416, Oct. 2017.
- [41] J. Dai, J. Zhang, W. Zhang, and D. Grischkowsky, "Terahertz time-domain spectroscopy characterization of the far-infrared absorption and index of refraction of high-resistivity, float-zone silicon," *J. Opt. Soc. Amer. B, Opt. Phys.*, vol. 21, no. 7, pp. 1379–1386, 2004.
- [42] V. E. Rogalin, I. A. Kaplunov, and G. I. Kropotov, "Optical materials for the THz range," *Ultraviolet, Infr., Terahertz Opt. Spectrosc.*, vol. 125, no. 6, pp. 1053–1064, 2018.



CRISTIANO M. B. CORDEIRO received the Ph.D. degree from the University of Campinas (UNICAMP), Brazil. He was a Postdoctoral Researcher with the University of Bath, England. He is currently an Assistant Professor with the Institute of Physics, UNICAMP and the Head of the Specialty Optical Fiber Laboratory. The main research areas of the laboratory are the development and application of silica photonic crystal fibers, microstructured polymer optical fibers, and

micro/nanofibers. His topics of interest include exploring new fiber functionalities and the use of new technologies in the optical fiber area. Applications related with optical devices and fiber sensors are under investigation. He is the author of 70 journal publications, 50 communications in international conferences, a book chapter and eight patents. He chaired the first edition of the Workshop on Specialty Optical Fibers (WSOF), now in its 6th edition.

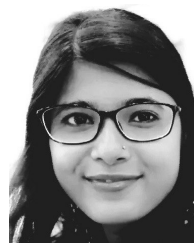


MD. J. NINE received the bachelor's degree from the Khulna University of Engineering & Technology, Bangladesh, in 2009, the Master of Engineering degree from Gyeongsang National University, South Korea, in 2012, and the Ph.D. degree in engineering on multifunctional coatings from The University of Adelaide, Australia. After his bachelor's degree, he joined in Second Phase of Brain Korea21 (BK21). He is currently an early-career Researcher based in ARC Research Hub for

Graphene Enabled Industry Transformation, The University of Adelaide, Australia. His current research interests involve synthesis and application of multifunctional inks and coatings based on 2D materials. The applications of coatings are including self-cleaning, corrosion resistant, fire-retardant, acoustic insulation, anti-bacterial, radiation shielding, and sensing. His research work has generated a number of items of intellectual property (IP) on graphene technology and one of them has already been licenced to an industry. He also serves as a member of extended advisory board of the *Carbon* journal, Elsevier. He was awarded a Doctoral Research Medal, Postgraduate Alumni University Medal, and *Carbon* journal Prize-2018 for outstanding research at Ph.D. level in The University of Adelaide.



MD. SAIFUL ISLAM (Member, IEEE) is currently pursuing the Ph.D. degree with the School of Electrical and Electronic Engineering, The University of Adelaide, Australia. He has published 39 peer-reviewed articles and actively reviews of the IEEE JOURNAL OF LIGHTWAVE TECHNOLOGY, the IEEE PHOTONICS JOURNAL, the IEEE SENSORS JOURNAL, the IEEE PHOTONICS TECHNOLOGY LETTERS, *Optics Express*, *Optics Letters*, *Applied Optics*, *Optical Material Express*, IEEE ACCESS, and *Scientific Reports*. His research interests include optical fiber communication, PCF based terahertz waveguides, terahertz sensors, surface plasmon resonance biosensors, topological insulators, and metamaterials for sensing applications. He is a member of the IEEE Young Professionals, Optical Society of America (OSA), and the Institute for Photonics & Advanced Sensing (IPAS).



JAKEYA SULTANA received the B.Sc. Engg. degree from the Rajshahi University of Engineering & Technology, in 2014, and the M.Sc. degree in engineering from the Islamic University of Technology, Bangladesh, in 2017. She is currently pursuing the Ph.D. degree with the School of Electrical and Electronic Engineering, The University of Adelaide, Australia. She is an Active Reviewer of the JOURNAL OF LIGHTWAVE TECHNOLOGY, the IEEE PHOTONIC TECHNOLOGY LETTER, *Optik*, and *Optical Communications*. Her research interests include anti-resonant fibers for terahertz application and super-continuum generation.



ALICE L. S. CRUZ was born in Sao Paulo, Brazil. She received the B.Eng. degree in automation engineering from Braz Cubas University, Mogi das Cruzes, Brazil, in 2011, and the M.Sc. and Ph.D. degrees in science from the Aeronautics Institute of Technology, Sao Jose dos Campos, Brazil, in 2014 and 2019, respectively. She has held a Lecturer position at Braz Cubas University.



ALEX DINOVTSER (Member, IEEE) is currently a Postdoctoral Fellow with The University of Adelaide, Australia. He has worked within the electronics manufacturing industry, designing computer interface, and signal acquisition systems. In 2008, he built the first spectroscopic lidar in Australia for the differential absorption detection of atmospheric trace gasses. Dr. Dinovtser is also a member of the Optical Society of America (OSA) and Engineers, Australia.



BRIAN WAI-HIM NG (Member, IEEE) is currently a Senior Lecturer with the School of Electrical and Electronic Engineering, The University of Adelaide. His research interests include radar signal processing, and wavelets and terahertz (T-ray) signal processing. Dr. Ng is also an Active Member within the South Australian Chapter of the IEEE. He was awarded The University of Adelaide Medal for the Top Graduate in Electrical and Electronic Engineering.



HEIKE EBENDORFF-HEIDEPRIEM received the Ph.D. degree from the University of Jena, Germany, in 1994. From 2001 to 2004, she was with the Optoelectronics Research Centre, University of Southampton, U.K. Since 2005, she has been with The University of Adelaide, Australia. She is currently the Deputy Director of the Institute for Photonics and Advanced Sensing. Her research focuses on the development of novel optical glasses, specialty optical fibres, surface functionalization, and sensing approaches. She received the Weyl International Glass Science Award and the prestigious Marie Curie Individual Fellowship, in 2001.



DUSAN LOSIC received the Ph.D. degree in nanoscience and nanotechnology from Flinders University, Australia, in 2003. He is currently a Professor with the School of Chemical Engineering, The University of Adelaide, Australia, and the Director of the Australian Research Council (ARC) Graphene Hub for Enabled Industry Transformation. He has published three books, 20 book chapters, >300 journal articles (14 journal covers), >80 conference papers, >150 conference presentations, eight patents, and six licensed technologies. He is also leading Nano Research group of >20 researchers and the ARC Graphene Hub >40 researchers. His interdisciplinary research in nanoscience and nanotechnology is focused on engineering new materials including graphene and their applications to address health, environmental, energy and agricultural problems. He received several Australian prestigious fellowships, the ARC Research Fellowship and ARC Future Fellowship.



DEREK ABBOTT (Fellow, IEEE) was born in London, U.K., in 1960. He received the B.Sc. degree (Hons.) in physics from Loughborough University, Loughborough, U.K., in 1982, and the Ph.D. degree in electrical and electronic engineering from The University of Adelaide, Adelaide, SA, Australia, in 1995, under K. Eshraghian and B. R. Davis. His interests are in the area of multidisciplinary physics and electronic engineering applied to complex systems. His research programs span a number of areas of stochastics, game theory, photonics, biomedical engineering, and computational neuroscience. Prof. Abbott is a Fellow of the Institute of Physics, U.K., and an Honorary Fellow of Engineers, Australia. He received number of awards, including the South Australian Tall Poppy Award for Science, in 2004, the Premier's SA Great Award in Science and Technology for outstanding contributions to South Australia, in 2004, an Australian Research Council Future Fellowship, in 2012, the David Dewhurst Medal, in 2015, the Barry Inglis Medal, in 2018, and the M. A. Sargent Medal, in 2019. He has served as an Editor and/or Guest Editor for a number of journals, including the IEEE JOURNAL OF SOLID STATE CIRCUITS, the *Journal of Optics B*, *Microelectronics Journal*, *Chaos*, *Smart Structures and Materials*, *Fluctuation and Noise Letters*, the PROCEEDINGS OF THE IEEE, and the IEEE PHOTONICS JOURNAL. He is on the editorial boards of *Scientific Reports* (Nature), *Royal Society Online Science*, and *Frontiers in Physics*. He is also the Editor-in-Chief (EIC) of IEEE ACCESS.

...